JOURNAL OF THE AMERICAN COLLEGE OF CARDIOLOGY VOL. 66, NO. 2, 2015

ISSN 0735-1097/$36.00
PUBLISHED BY ELSEVIER INC. http://dx.doi.org/10.1016/j.jacc.2015.05.008

Impact of Side Branch Modeling on Computation of Endothelial Shear Stress in Coronary Artery Disease

Coronary Tree Reconstruction by Fusion of 3D Angiography and OCT

Yingguang Li, MSc,* Juan Luis Gutiérrez-Chico, MD, PhD,† Niels R. Holm, MD,‡ Wenjie Yang, MD,§ Lasse Hebsgaard, MD,‡ Evald H. Christiansen, MD, PhD,‡ Michael Mæng, MD, PhD,‡ Jens F. Lassen, MD, PhD,‡ Fuhua Yan, MD,§ Johan H.C. Reiber, PhD,* Shengxian Tu, PhD‖

ABSTRACT

BACKGROUND Computational fluid dynamics allow virtual evaluation of coronary physiology and shear stress (SS). Most studies hitherto assumed the vessel as a single conduit without accounting for the flow through side branches.

OBJECTIVES This study sought to develop a new approach to reconstruct coronary geometry that also computes outgoing flow through side branches in hemodynamic and biomechanical calculations, using fusion of optical coherence tomography (OCT) and 3-dimensional (3D) angiography.

METHODS Twenty-one patients enrolled in the DOCTOR (Does Optical Coherence Tomography Optimize Revascularization) fusion study underwent OCT and 3D-angiography of the target vessel (9 left anterior descending, 2 left circumflex, 10 right coronary artery). Coronary 3D reconstruction was performed by fusion of OCT and angiography, creating a true anatomical tree model (TM) including the side branches, and a traditional single-conduit model (SCM) disregarding the side branches.

RESULTS The distal coronary pressure to aortic pressure (Pd/Pa) ratio was significantly higher in TMs than in SCMs (0.904 vs. 0.842; $p < 0.0001$). Agreement between TM and SCM in identifying patients with a Pd/Pa ratio ≤0.80 under basal flow conditions was only $k = 0.417$ ($p = 0.019$). Average SS was 4.64 Pascal lower in TMs than in SCMs ($p < 0.0001$), with marked differences in the point-per-point comparison, ranging from -60.71 to 7.47 Pascal.

CONCLUSIONS True anatomical TMs that take into account the flow through side branches are feasible for accurate hemodynamic and biomechanical calculations. Traditional SCMs underestimate Pd/Pa and are inaccurate for regional SS estimation. Implementation of TMs might improve the accuracy of SS and virtual fractional flow reserve calculations, thus improving the consistency of biomechanical studies. (J Am Coll Cardiol 2015;66:125–35) © 2015 by the American College of Cardiology Foundation.

From the *Division of Image Processing, Department of Radiology, Leiden University Medical Center, Leiden, the Netherlands; †Interventional Cardiology Department, Charité Medical University - Campus Benjamin Franklin, Berlin, Germany; ‡Department of Cardiology, Aarhus University Hospital, Skejby, Aarhus, Denmark; §Department of Radiology, Rui Jin Hospital, Shanghai Jiao Tong University School of Medicine, Shanghai, China; and the ‖Biomedical Instrument Institute, School of Biomedical Engineering, Shanghai Jiao Tong University, Shanghai, China. This work was supported in part by the Natural Science Foundation of China under Grant 61271155 and by Aarhus University Hospital and the PCI research group. Dr. Li is employed by Medis medical imaging systems BV; and has a research appointment at the Leiden University Medical Center. Dr. Holm receives speaker fees and research grants from St. Jude Medical and Terumo; and has received a research grant from Medis. Dr. Hebsgaard has received travel grants from Terumo and St. Jude Medical. Dr. Christiansen has received speaker fees and research grants from St. Jude Medical; and has received research grants from Terumo. Dr. Lassen has research grants from Terumo and St. Jude Medical. Dr. Reiber is the CEO of and holds equity in Medis medical imaging systems BV; and has a part-time appointment at Leiden University Medical Center

ABBREVIATIONS AND ACRONYMS

3D = 3-dimensional

CFD = computational fluid dynamics

FFR = fractional flow reserve

OCT = optical coherence tomography

Pd/Pa = distal coronary pressure to aortic pressure ratio

PCI = percutaneous coronary intervention

QCA = quantitative coronary angiography

SCM = single-conduit model

SS = shear stress

TM = tree model

Intracoronary shear stress (SS) is a potent stimulus for the endothelium, thus playing a relevant role in atherogenesis and plaque distribution within the vessel (1,2). Regions exposed to low SS are more prone to plaque progression, whereas in regions exposed to high SS atherogenesis is minimal (1,3,4). Uneven regional distribution of SS might explain the uneven distribution of atheroma plaques in specific anatomic coronary settings, such as curved vessels or bifurcations (2,5–7).

SEE PAGE 136

SS also modulates the neointimal vascular response after stenting, which drives the neointimalization of the device. The local level of SS is inversely related to the thickness of neointima and oscillatory SS enhances a hyperplastic neointima (8). This association has been consistently described in bare metal stents (9), drug-eluting stents (10,11), and bioresorbable scaffolds (12). The mechanism has been mainly attributed to anatomical or procedural scenarios that promote uneven distribution of SS forces, such as curved stented segments (11), bifurcational stenting techniques (12–15), undersizing, and malapposition (16–20). Moreover, SS promotes platelet activation and thrombosis (21–23) through von Willebrand factor binding to glycoprotein (GP) Ib and GP IIb/IIIa receptors (21–23). Therefore, it should be regarded as potentially prothrombogenic in the presence of malapposition, undersizing, or any kind of protruding struts.

Regional mapping of SS might be an excellent predictor of both plaque progression and outcomes after stenting. It could potentially be used to guide the intervention, including the decision about the need for optimization after stent deployment, but the complex and time-consuming method of calculation of SS has hitherto prevented the implementation of SS in the clinical routine. Additionally, a recent review has challenged the SS hypothesis on atherogenesis, indicating inconsistencies between different studies, and unravelling that the more refined level of quantitative point-by-point comparison, the poorer the association between low SS and atheroma (24). A possible source for inaccuracy that could explain this inconsistency is the influence of side branches in SS calculations: most previous biomechanical studies have estimated SS using the geometric reconstruction of the main vessel and have assumed it as a watertight conduit without flow losses through side branches (2,4–6,8,9,11,20,21,23,25,26). However, several recent studies using computational fluid dynamics (CFDs) have indicated that the impact of lost flow in side branches is not negligible and might affect substantially the accuracy of the SS estimation (27,28).

Co-registration software enabling the spatial combination of 3-dimensional (3D) angiography and optical coherence tomography (OCT) represents a realistic opportunity to calculate intracoronary biomechanics routinely in the catheterization lab in an accurate and time-efficient manner (29–31). For the current study we developed a novel method for calculation of SS that takes into account the flow lost through side branches, on the basis of the reconstruction of the coronary tree anatomy by fusion of 3D-OCT of the main vessel and 3D-angiography of the side branches. The impact of side branches on the accuracy of SS calculation is then evaluated in a clinical sample of real-world patients and compared to classical single-conduit methods.

METHODS

STUDY POPULATION. The Does Optical Coherence Tomography Optimize Revascularization (DOCTOR) fusion study was a prospective, single-arm, pilot study whose primary aim was exploring the feasibility of OCT-angiography co-registration and its potential to guide the percutaneous coronary intervention (PCI) (31). The current biomechanical study corresponds to the patients recruited in DOCTOR fusion. Patients were enrolled in a single center (Aarhus University Hospital, Skejby, Denmark). All patients who were referred for elective or urgent PCI between February 2013 and September 2013 were screened. Exclusion criteria included lesion length $>$ 40 mm (visually estimated), $>$ 2 lesions requiring PCI, serum creatinine $>$100 μmol/l, ST-segment elevation myocardial infarction within 7 days, cardiogenic shock, or severely tortuous vessels. The study was conducted according to the Declaration

(LUMC) as a Professor of Medical Imaging. Dr. Tu had an employment contract with Medis until June 2014; Shanghai Jiao Tong University receives institutional grant support on behalf of Dr. Tu from Medis. All other authors have reported that they have no relationships relevant to the contents of this paper to disclose. Drs. Li and Gutiérrez-Chico contributed equally to this work.
Listen to this manuscript's audio summary by *JACC* Editor-in-Chief Dr. Valentin Fuster.

Manuscript received January 31, 2015; revised manuscript received April 6, 2015, accepted May 4, 2015.

of Helsinki and the study was approved by the Mid-Jutland Committee for Biomedical Research and the Danish Data Protection Agency.

FUSION OF 3D ANGIOGRAPHY AND OCT. X-ray angiographic images were recorded with a flat-panel x-ray system (AlluraXper, Philips Healthcare, Best, the Netherlands). For each patient, the coronary artery with the most clinically relevant or most severe stenosis was selected as target vessel. Two angiographic projections with a difference in angulation >25° were obtained for the target vessel, including the whole course of all side branches of >1 mm diameter. On the basis of these 2 angiographic projections, a 3D reconstruction of the coronary segment comprising the whole stenotic length of the main vessel and the corresponding side branches was performed offline in a corelab (ClinFact, Leiden, the Netherlands) using a validated 3D quantitative coronary angiography (QCA) software package (QAngio XA 3D Research Edition 1.0, Medis Special BV, Leiden, the Netherlands) (28,29). Proximal and distal non-stenotic margins, with the corresponding side branches, were also included in the reconstruction.

OCT images of the target vessel were acquired with a Fourier-domain OCT system (Ilumien, St. Jude Medical, Inc., St. Paul, Minnesota) with a Dragonfly catheter (St. Jude Medical, Inc.) with nonocclusive technique (32) at an automated pullback speed of 20 mm/s and a frame rate of 100 Hz. The OCT pullback was co-registered and fused with the 3D angiography, using side branches as landmarks to correct for longitudinal and rotational mismatch due to cardiac motion artefacts or to random axial rotation of the catheter during OCT acquisition (30) (**Figure 1**). The fusion procedure relies on the identification of the side branch ostia in both the lumen contour of the OCT images and in the 3D angiography with subsequent calculation of their longitudinal positions and transversal angulations. Then the 3D-angiography luminogram of the main vessel is replaced by the 3D-OCT luminogram by matching their corresponding lumen centerlines. The correction for longitudinal and rotational mismatch of the OCT lumen succeeds after matching the side branch ostia with those of 3D angiography, and correcting the longitudinal positions and rotation of the non-matched cross sections by interpolation.

After fusion of the OCT and 3D-angiography images, 2 different geometrical models of the coronary lumen were generated:

1. A classical single-conduit model (SCM), consisting of the OCT lumen of the main vessel in a true 3D reconstruction on the basis of the fusion with the 3D angiography, disregarding the side branches.

FIGURE 1 Correction of Longitudinal and Rotational Mismatch During the Fusion of the OCT Pullback With 3D Angiography Using Side Branches as Landmarks

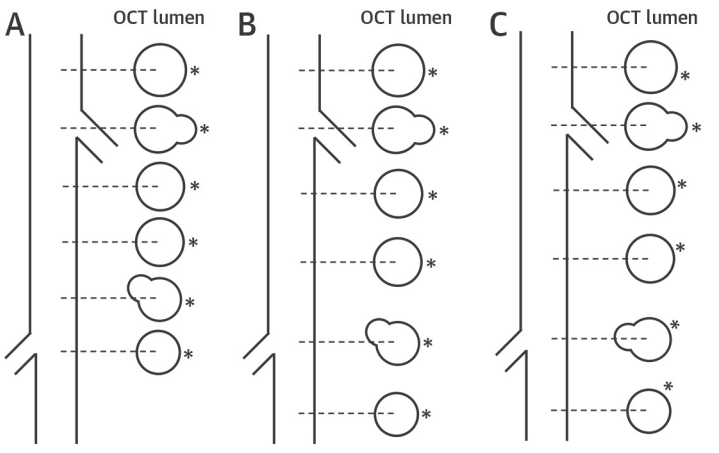

(A) Longitudinal and rotational mismatch between 3D angiography and OCT in axial position. **(B)** Correction of the longitudinal mismatch. **(C)** Correction of the rotational mismatch. Note that all frame rotations were interpolated between landmarks.
3D = 3 dimensional; OCT = optical coherence tomography.

2. A novel coronary tree model (TM), resulting of merging the lumen of the main vessel derived from OCT, as described in the SCM, with the lumina of the side branches derived from the 3D angiography (**Figure 2**, **Central Illustration**).

Both models were exported into separate stereolithography files for CFD analysis.

ANALYSIS OF ENDOTHELIAL SHEAR STRESS. The 3D reconstructed geometries were discretized using ANSYS ICEM 15.0 (ANSYS, Inc., Canonsburg, Pennsylvania) with tetrahedral cells (meshing). Volume tetrahedral meshes consisting of approximately 200,000 to 2 million tetrahedral elements were created for each model. Navier Stokes equations were implemented in each cell and nonlinear partial differential equations were solved simultaneously using ANSYS FLUENT 15.0 (ANSYS, Inc.). A blood density of 1,060 kg/m^3 and viscosity of 0.0035 kg/(m · s) were applied. No-slip condition was applied for the lumen wall. The mean volumetric flow rate was calculated from the volumetric coronary 3D rendering and the contrast transport time estimated by frame count in the angiography and applied at the inlet of the system (28). Assuming steady flow conditions, a fixed pressure of 13,332 Pascal was applied at the inlet boundary, whereas the fully developed flow condition was applied at the outflow boundaries. Vessel diameter and bifurcation angle as assessed by 3D angiography were used to determine the flow separation at

FIGURE 2 Geometrical Reconstruction in the Tree Model of an RCA and Computation of Endothelial SS

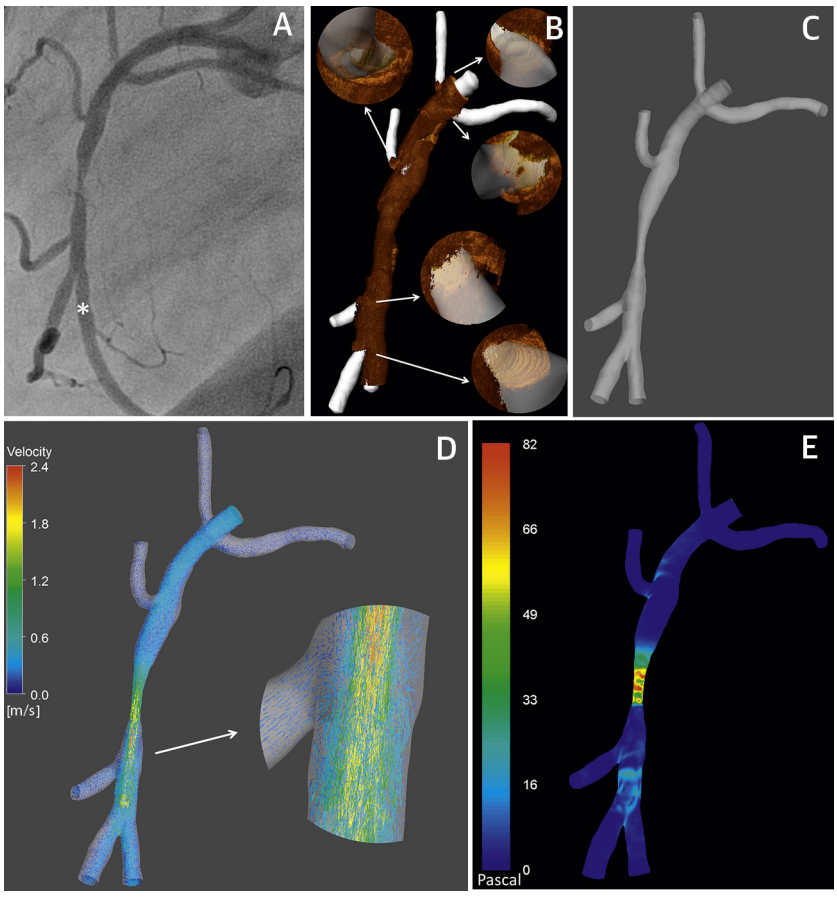

(A) Angiography of an RCA, with an OCT pullback starting at *. **(B)** Fusion of 3D angiography and OCT luminogram, using side branches (zoomed) as landmarks to correct for longitudinal and rotational mismatch. **(C)** Coronary tree model resulting from merging the OCT of the RCA with the 3D angiography of the side branches. **(D)** Simulated flow velocity. **(E)** Regional map of computed endothelial SS. CFD = computational fluid dynamics; RCA = right coronary artery; SS = shear stress; other abbreviations as in Figure 1.

the bifurcation (28). Finite volume method and parallel computing were used in the computation.

Meshing and CFD were performed separately on the SCMs and TMs, applying the same boundary conditions at the inlet. For the point-per-point comparison between the models, the main vessel lumen was divided in portions of 3-mm length and the width corresponding to an arc of 30° from the optic catheter (25,26). Mean endothelial SS within each portion was calculated in both models and matched for point-per-point comparison (**Central Illustration**). To minimize the bias due to the obvious differences in the velocity profile at the bifurcation core and to focus on the effect over straight coronary segments, cross sections involving the take-off of side branches were excluded from the comparison.

STATISTICS. Gaussian distribution of continuous variables was tested with the Kolmogorov-Smirnov test, and summarized as mean ± SD or as median (interquartile range as appropriate). Categorical variables were presented as counts (percentages). Comparison of continuous variables was performed with the Student *t* test for paired data or with the nonparametric Wilcoxon-W test, depending on their distribution. Because the study was primarily focused on SS, no angiography under maximal hyperemia was acquired; therefore, the agreement between TM and SCM for assessment of functional significance of stenoses could not be properly performed. Nonetheless, the agreement between TM and SCM for discrimination between distal coronary pressure and aortic pressure ratio (Pd/Pa) ≤0.80 versus >0.80

under basal flow conditions was assessed with the kappa coefficient. In terms of virtual fractional flow reserve (FFR), these values should correspond to the basal pressure ratio obtained under ordinary flow conditions before inducing maximal hyperemia with adenosine (28).

The point-per-point comparison of SS values was performed with a generalized linear mixed model pairwise, calculating the matrix of covariances of a hierarchical model with 3 levels: patient, longitudinal segment, and circumferential sector, to correct for the interdependence of clustered data. All statistical analyses were performed with IBM SPSS software (version 22.0, SPSS, Inc., Chicago, Illinois).

RESULTS

A total of 22 patients were included in the DOCTOR fusion study. One patient was excluded from the biomechanical study because OCT pre-stenting was not acquired, resulting in 21 patients in the final analysis. Lesion locations were: 9 left anterior descending (LAD), 2 left circumflex (LCX), and 10 right coronary artery (RCA). **Table 1** summarizes the baseline clinical and angiographic characteristics of patients and lesions, respectively. A mean of 1.57 side branches were identified in the target vessels, ranging from 0 to 4 (**Figure 3**). Four target vessels (2 LAD, 2 RCA) had no major side branch in the selected segment.

Table 2 and **Figure 4** summarize the comparison of hemodynamic variables between the 2 computational methods. The mean volumetric flow rate computed by 3D QCA and Thrombolysis In Myocardial Infarction (TIMI) frame count was 1.88 ± 0.84 ml/s and it was applied at the inlet boundaries of the TM and the SCM. The estimated outflow at the outlet boundary of the main vessel was significantly lower in the TM than in the SCM (1.377 vs. 1.894 ml/s; $p < 0.0001$). This subsequently resulted in significantly higher estimated pressure at the outlet boundary (Pd) of the main vessel (12,015.7 vs. 11,201.9 Pascal; $p < 0.0001$) and higher Pd/Pa ratio (0.904 vs. 0.842; $p < 0.0001$) for the TMs and SCMs, respectively. The same results were replicated in a stratified analysis by coronary artery, although the difference tended to be more pronounced in the LAD (mean difference in outflow: -0.66 ml/s; 95% confidence interval [CI] -1.08 to -0.24 ml/s; $p = 0.007$) and softer in the RCA (mean difference in outflow: -0.35; 95% CI -0.60 to -0.09; $p = 0.014$) (**Figure 5**). Six patients had a Pd/Pa ratio ≤0.8 in basal flow conditions according to the SCM, but this finding was confirmed only in 2 of them by the anatomical tree model (kappa 0.417; $p = 0.019$).

For the biomechanical point-per-point comparison, the coronary segments were subdivided in 2,532 portions. After exclusion of the cross sections that involved the take-off of side branches, only 1,920 portions remained for the comparison. The histogram of frequencies shows the distribution of the paired differences in SS (**Figure 6**). In 545 portions (28.4%), both methods resulted in similar calculation of SS (-0.5 Pascal ≤ difference ≤0.5 Pascal), in 1,184 portions (61.7 %) the TM resulted in >0.5 Pascal lower SS calculation than the classical SCM, whereas in 191 portions (9.9%) the TM resulted in >0.5 Pascal higher SS than the SCM. In an unclustered pairwise comparison, the differences in SS between the TM and the SCM ranged from -60.71 to 7.47 Pascal. In the hierarchical generalized linear mixed model pairwise, SS in the TM was on average 4.64 Pascal lower than in the SCM ($p < 0.0001$).

DISCUSSION

The main findings of this study can be summarized as follows: 1) True anatomical reconstruction of a coronary artery and its side branches (tree model) is feasible by fusion of the OCT luminogram of the target artery and the 3D-angiography luminograms of the side branches. 2) Coronary TMs enable precise hemodynamic and biomechanical calculations, taking into account the flow lost through the side branches. 3) Compared with true anatomical TMs, the classical SCM underestimate significantly the Pd/Pa ratio of the lesion and render inaccurate regional SS calculations: overestimated in 61.7% and underestimated in 9.9% of the coronary portions.

These results are consistent with a previous exploratory study performed on 17 RCAs (5 of them with coronary heart disease) using 3D angiography: the inclusion or exclusion of side branches caused differences in flow through the main vessel up to 78.7% and in SS values of up to 12 Pascal (27). The sample of the current study included all types of coronary vessels, not only the RCA, in which the effect of the side branches is not so pronounced as in other coronary vessels such as the LAD. Furthermore, the lumen reconstruction of the main vessel in the current study was on the basis of OCT, thus enabling a level of detail much higher than a simple 3D angiography. Finally, whereas the CFD in the previous study determined flow separation solely by vessel diameter, the current study used both vessel diameter and bifurcation angle to determine flow separation, a strategy that had been previously validated using invasive FFR measurement (28).

CENTRAL ILLUSTRATION **Geometrical Reconstruction of a Left Anterior Descending Artery and Differences of Shear Stress Computation Between the Novel Tree Model and the Classical Single-Conduit Model**

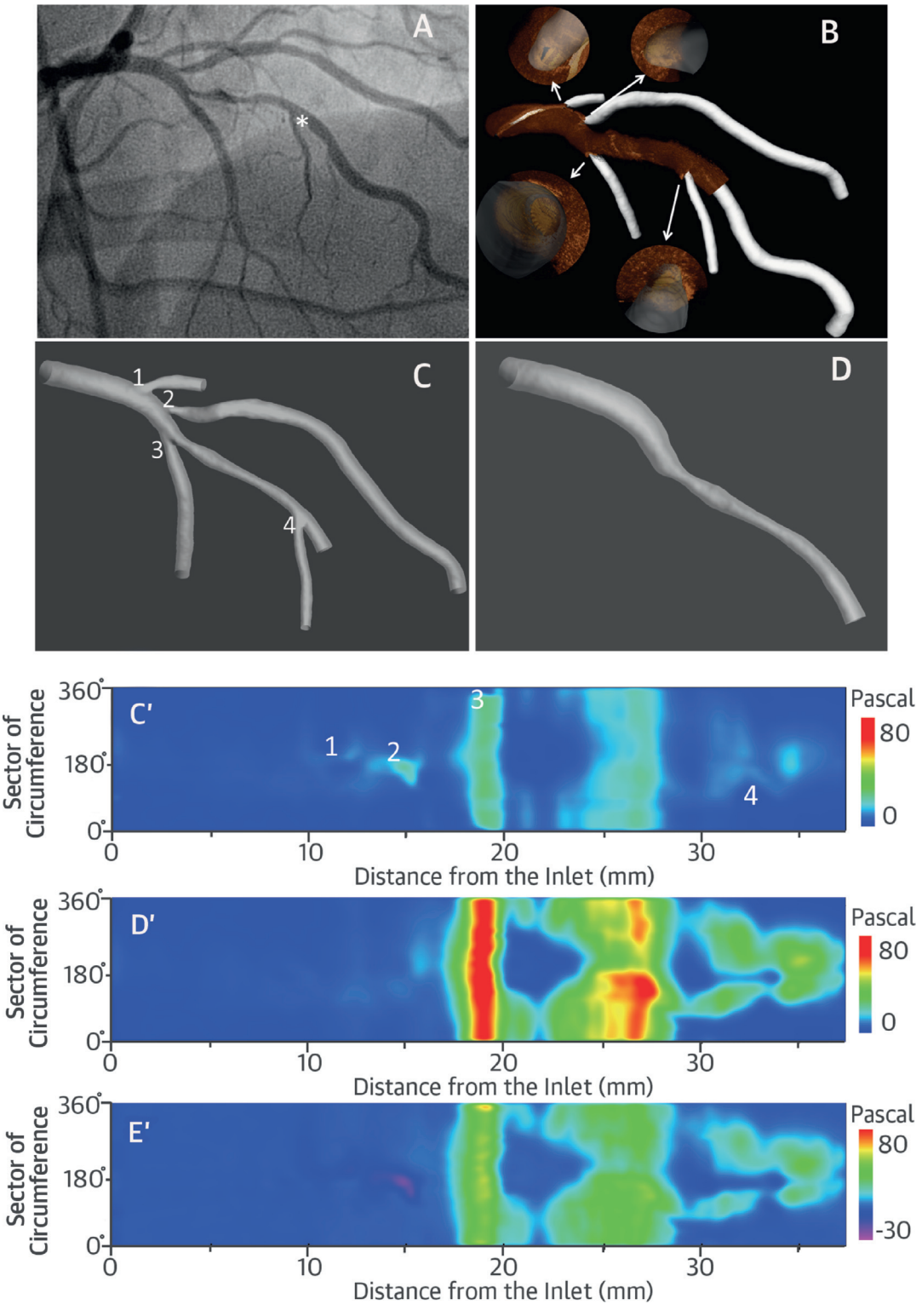

Li, Y. et al. J Am Coll Cardiol. 2015; 66(2):125–35.

Continued on the next page

TABLE 1 Baseline Clinical and Angiographic Characteristics of the Patients and Lesions Included for Analysis in the Study

Clinical and Angiographic Characteristics	(n = 21)
Male	17 (81.0)
Age, yrs	60.0 (52.5-69.5)
Hypertension	12 (57.1)
Hypercholesterolemia	12 (57.1)
Diabetes mellitus	2 (9.5)
Smoker	
Previous smoker	8 (38.1)
Current smoker	4 (19.0)
Prior PCI	4 (19.0)
Indication for coronary angiography	
Stable angina	13 (61.9)
Unstable angina	1 (4.8)
NSTEMI	7 (33.3)
Coronary vessel	
LAD	10 (47.6)
LCX	2 (9.5)
RCA	9 (42.9)
% Diameter stenosis (QCA)	69 ± 10
Calcified lesion	4 (19.0)
Number of side branches	1.57 ± 1.08

Values are n (%), median (interquartile range), or mean ± SD.

LAD = left anterior descending; LCX = left circumflex; NSTEMI = non-ST-segment elevation myocardial infarction; PCI = percutaneous coronary intervention; QCA = quantitative coronary angiography; RCA = right coronary artery.

FIGURE 3 Lumen Geometry in All Analyzed Cases

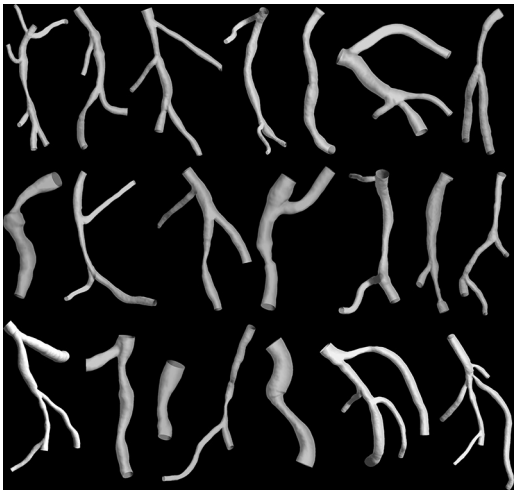

Lumen resulting from the fusion of OCT in the main vessel and 3D angiography in the coronary tree model. Abbreviations as in Figure 1.

To the best of our knowledge, the TM developed for this study is the only OCT-3D angiography fusion method to date that uses the 3D disposition of the side branches to correct for rotational mismatch. During the acquisition of an OCT pullback several factors can induce subtle uniform variations in the rotation speed of the optic catheter, thus resulting in some degree of torsion in the consecutive cross sections. This random axial rotation of the OCT images has been a source of inaccuracy for a real 3D reconstruction, hitherto technically very difficult to address. The TM uses the take-off of side branches in both OCT and 3D angiography to correct for this rotational mismatch, interpolating the rotation of cross sections between side-branches. This is a significant leap forward for the centerline-guided fusion method, which enabled reliable OCT-3D angiography co-registration, correcting for longitudinal mismatch between both techniques (28,29). With the correction for both longitudinal and rotational mismatches, the TM might render the closest representation to the true coronary anatomy on the basis of OCT imaging to date. Still other sources of image distortion, mainly the cardiac-motion artefact, remain to be addressed.

Regarding the hemodynamic calculations, the main consequence of switching the computational model is the change in magnitude of the estimated flow in the main vessel. The TM computes the flow through side branches, whereas the SCM does not. Therefore, according to the principles of conservation of mass and momentum, the estimated flow in the

CENTRAL ILLUSTRATION

(A) Angiography of a LM-LAD artery, with an optical coherence tomography pullback starting at *. **(B)** Fusion of 3D angiography and OCT luminogram, using side branches (zoomed) as landmarks to correct for longitudinal and rotational mismatch. **(C)** Novel coronary tree model resulting from merging the OCT of the LM-LAD with the 3D angiography of the side branches. Numbers indicate the 4 bifurcations involved. **(D)** Classical single-conduit model, on the basis of the true 3D reconstruction of the OCT lumen of the main vessel, disregarding the side branches for the CFD simulation. **(C' and D')** Spread-out vessel map of the SS distribution, with the distance from the ostium of the main vessel in the x-axis and the circumference location within the cross section in the y-axis, for both the coronary tree **(C')** and the single-conduit **(D')** models. **Numbers** correspond to the 4 bifurcations shown in **C**. **(E')** Difference in SS values between both models (single conduit − tree). The outflow in the LAD calculated by the tree and by the single-conduit models was 0.65 ml/s and 1.16 ml/s, respectively, resulting in simulated pressure drops between the inlet and the outlet of 734 Pascal and 1,405 Pascal, respectively. 3D = 3 dimensional; CFD = computational fluid dynamics; LAD = left anterior descending; LM = left main trunk; OCT = optical coherence tomography.

TABLE 2 Differences in Flow and Pressure in the Main Vessel Between the 2 Different Computational Models

			Difference			
				95% CI		
	Tree	Single-Conduit	Mean	Lower	Upper	p Value
Outflow (ml/s)	1.377	1.894	−0.517	−0.724	−0.310	<0.0001
Pd (Pascal)	12,015.7	11,201.9	813.8	NA	NA	<0.0001*
Pd/Pa	0.904	0.842	0.062	NA	NA	<0.0001*

*Wilcoxon signed ranked test for paired data.

CI = confidence interval; NA = no applicable; Pa = pressure estimated at the inlet; Pd = pressure estimated at the outflow boundary in the main vessel.

main vessel will be always smaller in the TM than in the SCM. Because the pressure drop through a stenosis is directly proportional to the flow through it, the estimated distal pressures (Pd) and the corresponding Pd/Pa ratios will be higher in the TM than in the SCM. In the example shown in the **Central Illustration**, the outflow in the main vessel was 0.65 ml/s as calculated by the TM, but 1.16 ml/s as calculated by the SCM, resulting in significantly different pressure drops across the stenosis: 734 Pascal versus 1405 Pascal, respectively. This difference between models is not negligible because disregarding the flow through side branches reduces the specificity of the virtual estimation of Pd/Pa. In our study, 66.66% of the lesions considered functionally significant in basal flow conditions (Pd/Pa ≤0.8) by the traditional SCM were not confirmed after incorporating the side branches into the computation. The agreement for this binary classification between both computational methods was as low as kappa = 0.417, even though all the other variables were identical. This information is clinically relevant for non-invasive and virtual FFR calculation on the basis of CFD and coronary imaging (28-30,33). The agreement between TM and SCM for a proper virtual FFR under hyperemic conditions could not be properly reported because the clinical protocol was primarily designed for SS calculation, so no adenosine was administered and no TIMI frame count under hyperemia was obtained. The influence of the computational mode on virtual FFR needs to be defined in forthcoming studies.

FIGURE 4 Differences in Outflow and Estimated Pressures in the Coronary Tree and Single-Conduit Models

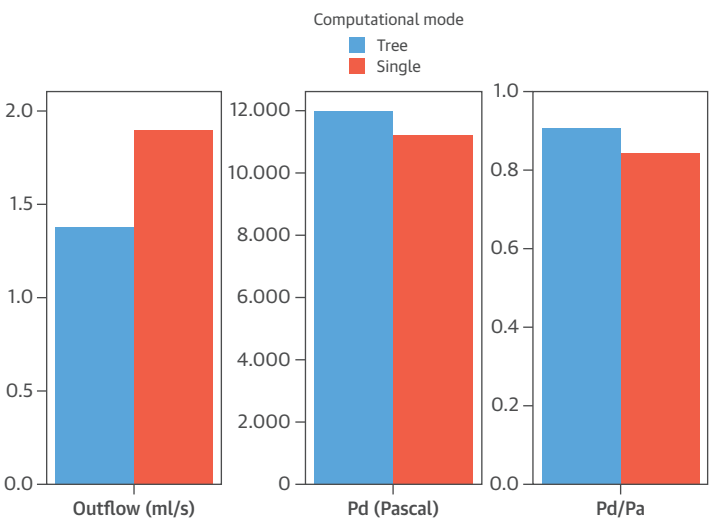

Pa = pressure estimated at the inlet of the system; Pd = pressure estimated at the outlet boundary of the main vessel.

Regarding the SS calculation, 2 major factors explain our findings: 1) the change in flow magnitude in the main vessel; and 2) the directionality of the flow diverted through the side branches, resulting in regional changes in the flow pattern, i.e., the shift of the center of the parabolic laminar flow from the center of the cross section towards a lateral wall. Although the decrease of flow magnitude generally decreases the SS for the entire cross section in the TM, the change of flow pattern can lead to an increase or decrease of the SS depending on the location of the regions. The combination of these 2 factors explains the average lower estimation of SS in the TM, but the higher SS at some regions (9.9%), normally in the vicinity of the SB take-off or in tortuous segments, due to changes of the flow pattern in the CFD simulation. Additionally, in 28.4% of the portions, the TM resulted in similar SS calculation to the classical SCM: this could be expected in the 4 cases with no side branch and in coronary segments proximal to the bifurcations, in which the hemodynamic conditions of both models are identical, but also in segments distant from bifurcations and stenosis, in which the overall reduction in flow magnitude was compensated by changes in the flow pattern, resulting in similar SS values. Previous publications had already suggested that the incorporation of side braches to the computation would affect the SS values obtained far from bifurcation or stenosis (27). The relevance of our findings is best depicted in the **Central Illustration**: the traditional SCM is simply inaccurate for SS calculation. The statistical comparison is indeed irrelevant in light of the evidence that the regional estimation of SS can be overestimated by up to 60.71 Pascal or underestimated by up to 7.47 Pascal under the assumption that the coronary flow happens in a watertight conduit without side branches. This approach has been the conventional method to

FIGURE 5 Differences in Outflow Between the 2 Computational Models (Tree vs. Single-Conduit), Stratified by Coronary Artery

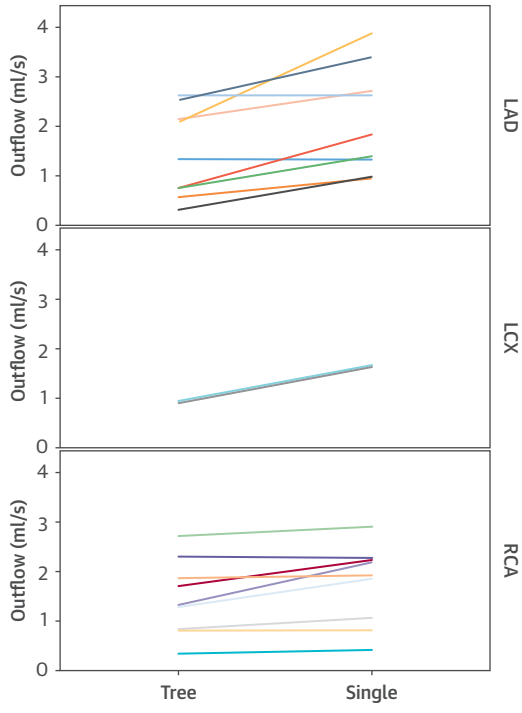

LAD = left anterior descending; LCX = left circumflex; RCA = right coronary artery.

FIGURE 6 Histogram of Frequencies Showing the Distribution of the Point-Per-Point Difference in Shear Stress Between the 2 Computational Models (Tree – Single Conduit)

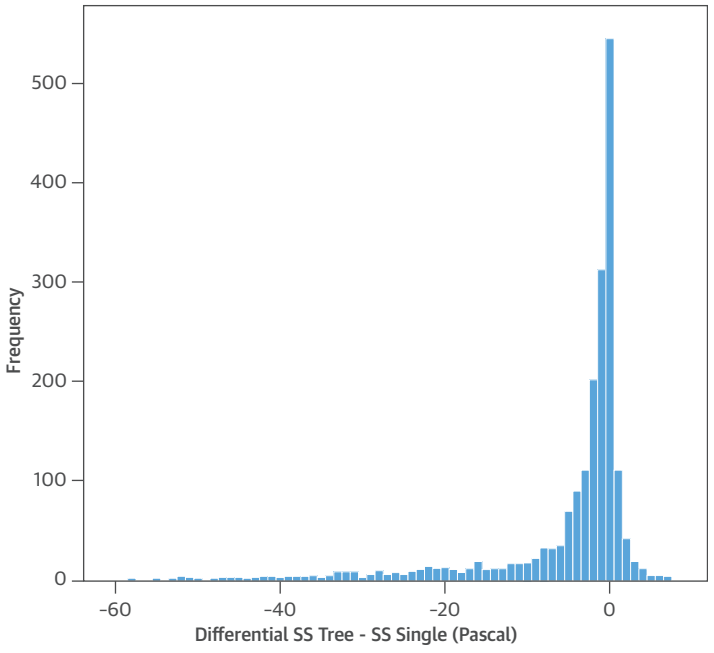

SS = shear stress.

calculate SS (2,4-6,8,9,11,20,21,23,25,26) and a reasonable approximation because the incorporation of side branches has been technically too complex. Nonetheless, the extraordinary development of 3D angiography, OCT, and CFD now permits to overcome this limitation (29,30) by incorporating the side branches in a TM to refine SS calculations.

The relative simplicity of this TM opens the door to its implementation in large-scale clinical studies that might contribute to define the role of biomechanics in different clinically relevant processes, such as atherogenesis, restenosis, or healing after stenting, currently under debate (24). Indeed our study unravels inaccuracies of the classical SCM for SS computation that might partially explain the apparent discrepancy between different studies (24). Revisiting previous publications from this novel perspective might help to understand the conflicting data and might strengthen the consistency of future studies on this field.

STUDY LIMITATIONS. The patients in our study were referred for elective or urgent PCI. The extrapolation of these results to a population with milder degrees or without coronary heart disease should be undertaken with caution because the magnitude of the effect of the TM might be different. Likewise, 4 patients in the sample had no side branch in the selected segment of the target vessel; therefore, their inclusion in this study might have buffered the effect of the computational model. Nonetheless, we decided to include them in the analysis because an important aim of this study was to estimate the impact of the computational mode on a sample of unselected patients to judge the relevance for future studies.

The luminogram of side branches stemming from 3D-QCA is only an oval approximation, whose cross-sectional area is probably slightly underestimated as compared with the area measured by OCT (34,35). This would be a major limitation if we intended to calculate the SS in the side branches; however, the aim of our study was simply estimating the outgoing flow through the side branches. For this aim, the cross-sectional area from 3D angiography should be accurate enough to make a reasonable estimation. Likewise, minor side branches (<1 mm caliber in angiography) still cannot be computed in the TM, so

they could be still a source for inaccuracy, even though the error is most likely small.

The point-per-point comparison in biomechanical studies is still very challenging. A recent systematic review unveiled that the correlation between SS and atherosclerosis increases for increasing levels of data reduction, but it is minimal at the point-per-point comparison (24). This finding emphasizes the regional matching as a challenge that jeopardizes the accuracy of biomechanical studies. However, the current study enabled a very accurate regional matching because the comparison was performed on 2 different models derived from the same OCT pullback and the same 3D reconstruction, with the only exception being the side branches. Therefore, the role played by an eventual regional mismatching is probably negligible, but cannot be completely ruled out.

CONCLUSIONS

True anatomical coronary TMs taking into account the flow through side branches are feasible by fusion of OCT and 3D coronary angiography, thus enabling accurate hemodynamic and biomechanical calculations in real-world patients. Traditional SCMs underestimate Pd/Pa ratios and are inaccurate for the calculation of regional SS estimation, with errors ranging between −7.47 and 60.71 Pascal. Implementation of TMs might improve the accuracy of SS estimation and virtual FFR calculations and avoid inconsistency between studies.

REPRINT REQUESTS AND CORRESPONDENCE: Dr. Shengxian Tu, Room 123, Med-X Research Institute, Shanghai Jiao Tong University, No. 1954, Hua Shan Road, Shanghai 200030, China. E-mail: sxtu@sjtu.edu.cn.

PERSPECTIVES

COMPETENCY IN MEDICAL KNOWLEDGE: Calculations on the basis of conventional single-conduit models overestimate intracoronary shear stress, and more accurate estimates can be derived by combining data from 3D coronary angiography, optical coherence tomography, and fluid dynamics.

TRANSLATIONAL OUTLOOK: Future studies of shear stress should account for outgoing flow through side branches to assure more accurate calculations to avoid overestimating the pressure drop across a stenotic lesion and underestimating fractional flow reserve.

REFERENCES

1. Malek AM, Alper SL, Izumo S. Hemodynamic shear stress and its role in atherosclerosis. JAMA 1999;282:2035–42.

2. Cheng C, Tempel D, van Haperen R, et al. Atherosclerotic lesion size and vulnerability are determined by patterns of fluid shear stress. Circulation 2006;113:2744–53.

3. Samady H, Eshtehardi P, McDaniel MC, et al. Coronary artery wall shear stress is associated with progression and transformation of atherosclerotic plaque and arterial remodeling in patients with coronary artery disease. Circulation 2011;124:779–88.

4. Chatzizisis YS, Jonas M, Coskun AU, et al. Prediction of the localization of high-risk coronary atherosclerotic plaques on the basis of low endothelial shear stress: an intravascular ultrasound and histopathology natural history study. Circulation 2008;117:993–1002.

5. Wentzel JJ, Janssen E, Vos J, et al. Extension of increased atherosclerotic wall thickness into high shear stress regions is associated with loss of compensatory remodeling. Circulation 2003;108:17–23.

6. Asakura T, Karino T. Flow patterns and spatial distribution of atherosclerotic lesions in human coronary arteries. Circ Res 1990;66:1045–66.

7. Tadjfar M. Branch angle and flow into a symmetric bifurcation. J Biomech Eng 2004;126:516–8.

8. Thury A, Wentzel JJ, Vinke RVH, et al. Focal in-stent restenosis near step-up: roles of low and oscillating shear stress? Circulation 2002;105:e185–7.

9. Wentzel JJ, Krams R, Schuurbiers JC, et al. Relationship between neointimal thickness and shear stress after Wallstent implantation in human coronary arteries. Circulation 2001;103:1740–5.

10. Tanabe K, Gijsen FJH, Degertekin M, et al. Images in cardiovascular medicine. True three-dimensional reconstructed images showing lumen after sirolimus-eluting stent implantation. Circulation 2002;106:e179–80.

11. Gijsen FJ, Oortman RM, Wentzel JJ, et al. Usefulness of shear stress pattern in predicting neointima distribution in sirolimus-eluting stents in coronary arteries. Am J Cardiol 2003;92:1325–8.

12. Karanasos A, Li Y, Tu S, et al. Is it safe to implant bioresorbable scaffolds in ostial side-branch lesions? Impact of 'neo-carina' formation on main-branch flow pattern. Longitudinal clinical observations. Atherosclerosis 2015;238:22–5.

13. Hu ZY, Chen SL, Zhang JJ, et al. Distribution and magnitude of shear stress after coronary bifurcation lesions stenting with the classical crush technique: a new predictor for in-stent restenosis. J Interv Cardiol 2010;23:330–40.

14. Moore JE Jr., Timmins LH, Ladisa JF Jr. Coronary artery bifurcation biomechanics and implications for interventional strategies. Catheter Cardiovasc Interv 2010;76:836–43.

15. Williams AR, Koo BK, Gundert TJ, et al. Local hemodynamic changes caused by main branch stent implantation and subsequent virtual side branch balloon angioplasty in a representative coronary bifurcation. J Appl Physiol 2010;109:532–40.

16. Kolandaivelu K, Swaminathan R, Gibson WJ, et al. Stent thrombogenicity early in high-risk interventional settings is driven by stent design and deployment and protected by polymer-drug coatings. Circulation 2011;123:1400–9.

17. Gutiérrez-Chico JL, Regar E, Nüesch E, et al. Delayed coverage in malapposed and side-branch struts with respect to well-apposed struts in drug-eluting stents. Circulation 2011;124:612–23.

18. Gutiérrez-Chico JL, Wykrzykowska JJ, Nüesch E, et al. Vascular tissue reaction to acute malapposition in human coronary arteries: sequential assessment with optical coherence tomography. Circ Cardiovasc Interv 2012;5:20–9.

19. Gutiérrez-Chico JL, Gijsen FJH, Regar E, et al. Differences in neointimal thickness between the

adluminal and the abluminal sides of malapposed and side-branch struts: evidence in vivo about the abluminal healing process. J Am Coll Cardiol Intv 2012;5:428–35.

20. Foin N, Gutierrez-Chico JL, Nakatani S, et al. Incomplete stent apposition causes high shear flow disturbances and delay in neointimal coverage as a function of strut to wall detachment distance: implications for the management of incomplete stent apposition. Circ Cardiovasc Interv 2014;7:180–9.

21. Holme PA, Orvim U, Hamers MJ, et al. Shear-induced platelet activation and platelet microparticle formation at blood flow conditions as in arteries with a severe stenosis. Arterioscler Thromb Vasc Biol 1997;17:646–53.

22. Badimon L, Badimon JJ, Turitto VT, et al. Platelet thrombus formation on collagen type I. A model of deep vessel injury. Influence of blood rheology, von Willebrand factor, and blood coagulation. Circulation 1988;78:1431–42.

23. Moake JL, Turner NA, Stathopoulos NA, et al. Shear-induced platelet aggregation can be mediated by vWF released from platelets, as well as by exogenous large or unusually large vWF multimers, requires adenosine diphosphate, and is resistant to aspirin. Blood 1988;71:1366–74.

24. Peiffer V, Sherwin SJ, Weinberg PD. Does low and oscillatory wall shear stress correlate spatially with early atherosclerosis? A systematic review. Cardiovasc Res 2013;99:242–50.

25. Vergallo R, Papafaklis MI, Yonetsu T, et al. Endothelial shear stress and coronary plaque characteristics in humans: combined frequency-domain optical coherence tomography and computational fluid dynamics study. Circ Cardiovasc Imaging 2014;7:905–11.

26. Stone PH, Saito S, Takahashi S, et al. Prediction of progression of coronary artery disease and clinical outcomes using vascular profiling of endothelial shear stress and arterial plaque characteristics: the PREDICTION Study. Circulation 2012;126:172–81.

27. Wellnhofer E, Osman J, Kertzscher U, et al. Flow simulation studies in coronary arteries—impact of side-branches. Atherosclerosis 2010; 213:475–81.

28. Tu S, Barbato E, Koszegi Z, et al. Fractional flow reserve calculation from 3-dimensional quantitative coronary angiography and TIMI frame count: a fast computer model to quantify the functional significance of moderately obstructed coronary arteries. J Am Coll Cardiol Intv 2014;7:768–77.

29. Tu S, Holm NR, Christiansen EH, et al. First presentation of 3-dimensional reconstruction and centerline-guided assessment of coronary bifurcation by fusion of X-ray angiography and optical coherence tomography. J Am Coll Cardiol Intv 2012;5:884–5.

30. Tu S, Pyxaras SA, Li Y, et al. In vivo flow simulation at coronary bifurcation reconstructed by fusion of 3-dimensional x-ray angiography and optical coherence tomography. Circ Cardiovasc Interv 2013;6:e15–7.

31. Hebsgaard L, Nielsen TM, Tu S, et al. Co-registration of optical coherence tomography and x-ray angiography in percutaneous coronary intervention. The Does Optical Coherence Tomography Optimize Revascularization (DOCTOR) Fusion Study. Int J Cardiol 2015;182:272–8.

32. Prati F, Cera M, Ramazzotti V, et al. Safety and feasibility of a new non-occlusive technique for facilitated intracoronary optical coherence tomography (OCT) acquisition in various clinical and anatomical scenarios. EuroIntervention 2007;3: 365–70.

33. Koo BK, Erglis A, Doh JH, et al. Diagnosis of ischemia-causing coronary stenoses by non-invasive fractional flow reserve computed from coronary computed tomographic angiograms. Results from the prospective multicenter DISCOVER-FLOW (Diagnosis of Ischemia-Causing Stenoses Obtained Via Noninvasive Fractional Flow Reserve) study. J Am Coll Cardiol 2011;58:1989–97.

34. Gonzalo N, Serruys PW, Garcia-Garcia HM, et al. Quantitative ex vivo and in vivo comparison of lumen dimensions measured by optical coherence tomography and intravascular ultrasound in human coronary arteries. Rev Esp Cardiol 2009; 62:615–24.

35. Gutierrez-Chico JL, Serruys PW, Girasis C, et al. Quantitative multi-modality imaging analysis of a fully bioresorbable stent: a head-to-head comparison between QCA, IVUS and OCT. Int J Cardiovasc Imaging 2012;28:467–78.

KEY WORDS computational fluid dynamics, fractional flow reserve, optical coherence tomography, shear stress